Journal of Power Sources 196 (2011) 4842–4848

Contents lists available at ScienceDirect

Journal of Power Sources

journal homepage: www.elsevier.com/locate/jpowsour

Electrodeposition and pseudocapacitive properties of tungsten oxide/polyaniline composite

Ben-Xue Zou [a,b], Ying Liang [a], Xiao-Xia Liu [a,*], Dermot Diamond [c], King-Tong Lau [c,**]

[a] China-Ireland Center for Advanced Materials and Sensor Development, Department of Chemistry, Northeastern University, Shenyang, 110004, China
[b] Department of Chemical engineering, Liaodong University, Dandong, 118000, China
[c] National Centre for Sensor Research, School of Chemical Sciences, Dublin City University, Glasnevin, Dublin 9, Ireland

ARTICLE INFO

Article history:
Received 6 November 2010
Received in revised form 20 January 2011
Accepted 21 January 2011
Available online 28 January 2011

Keywords:
Tungsten oxide
Polyaniline
Negative electrode material
Asymmetric capacitor

ABSTRACT

Composite films of tungsten oxide (WO_3) and polyaniline (PANI) have been electrodeposited by cyclic voltammetry in a mixed solution of aniline and precursor of tungsten oxide. Surface morphology and chemical composition of WO_3/PANI composite are characterized by scanning electron microscopy (SEM) and X-ray photoelectron spectroscopy (XPS). The influence of H_2O_2 on the electrodeposition of WO_3/PANI composite film is also investigated. Cyclic voltammetry (CV), chronopotentiometry (CP) and electrochemical impedance spectroscopy (EIS) results show that WO_3/PANI composite film exhibit good pseudocapacitive performance over a wide potential range of −0.5 to 0.7 V *vs.* SCE with the specific capacitance of 168 F g^{-1} at current density of 1.28 mA cm^{-2} and energy density of 33.6 Wh kg^{-1}, which is 91% higher than that of similarly prepared PANI (17.6 Wh kg^{-1}). An asymmetric model capacitor using WO_3/PANI as negative and PANI as positive electrodes over voltage range of 1.2 V displays a specific capacitance of 48.6 F g^{-1} and energy density of 9.72 Wh kg^{-1} at the power density of 53 W kg^{-1}, which is two times higher than that of a symmetric capacitor modeled by using two PANI films as both positive and negative electrodes.

1. Introduction

Electrochemical capacitors (ECs) have potential applications in electronic fuses, backup power sources and power delivery devices for electric vehicles [1–3]. Several transition metal oxides and conducting polymers are considered as promising materials for pseudocapacitors. Ruthenium oxide (RuO_2) gives appreciable specific capacitance of 600–1000 F g^{-1} over a wide potential range of 1.4 V [4]. However, high cost and toxicity limit its commercial applications. Some low cost metal oxides such as NiO, CoO_x and MnO_x etc. have been investigated as electrode materials for ECs [5–8]. Furthermore, various conducting polymers such as polyaniline (PANI), polypyrrole (PPy) and their derivatives have been widely studied due to their large specific capacitance [9,10]. However, most metal oxides and conducting polymers usually display electroactivities in narrow positive potential range in aqueous electrolyte, which resulted in limited operating voltage (V) of capacitors based on these electrode materials and low energy density (E_s) according to the equation $E_s = 1/2C_sV^2$.

Owing to large specific surface area, carbon materials have been widely employed as negative electrode for supercapacitors having a large operating voltage [11,12]. However, low specific capacitance of carbon is major limitation for application because its charges are just accumulated by electrical double-layer. Many efforts have been devoted to develop new materials for negative electrode. For instance, polythiophene-based conducting polymers have been intensively investigated in recent years, which display electroactivities in both positive and negative potentials due to p- and n-dopings, respectively. Supercapacitors assembled by these polymers as positive and negative electrode materials have a large operating voltage of 3 V [13,14]. However, the n-doping charge is only half of the p-doping charge, which, together with the poorer cycle stability of n-doping process, impedes the application of such electrode materials [15]. Redox polymer complexes have also been studied [16]. The polymer complexes of transition metals, in which the metal centers are in different oxidation states, are used for both positive and negative electrodes to increase operating voltage of the capacitor [16]. Owen and Brace discovered that a mesostructured titanium dioxide can be repeatedly reduced and reoxidized in aqueous lithium hydroxide and its reduction potential is close to that of hydrogen evolution so that it can be a candidate as negative electrode material for ECs with enlarged potential window [17].

Tungsten oxide (WO_3) is an attractive metal oxide which exhibits multiple oxidation states due to intercalation of electrons

* Corresponding author. Tel.: +86 24 83689510; fax: +86 24 23600159.
** Corresponding author. Tel.: +353 1 700 6008; fax: +353 1 700 7995.
E-mail addresses: xxliu@mail.neu.edu.cn (X.-X. Liu), Kim.lau@dcu.ie (K.-T. Lau).

0378-7753/$ – see front matter © 2011 Elsevier B.V. All rights reserved.
doi:10.1016/j.jpowsour.2011.01.073

and protons into the oxide to form hydrogen tungsten bronzes (H_xWO_3) and/or reduction of WO_3 to substoichiometric oxide (WO_{3-y}) through breaking of tungsten–oxygen bonds [18–20]. To reduce the cost of $RuO_2{\cdot}xH_2O$ based pseudocapacitive materials, tungsten oxide/ruthenium oxide composites were synthesized [21]. Although tungsten oxides showed little capacitance, an amorphous composite sample with 50 wt% tungsten content exhibited a specific capacitance of around 560 F g^{-1} which is 200 F g^{-1} higher than that as expected on the basis of the mixture. The high specific capacitance was ascribed to the participation of proton provided by the tungsten oxide. The pseudocapacitive properties of amorphous tungsten oxide synthesized by microwave irradiation have been investigated over the potential range of 0–0.5 V *vs.* SCE which displayed a volumetric capacitance of 231 F cm^{-3} [22]. Although tungsten oxide shows electroactivities over comparatively negative potential range [20], its pseudocapacitive properties over this negative potential range and used as negative electrode materials in supercapacitors have not been reported, as far as we know.

Recently, conducting polymer based organic-inorganic composite materials have been widely investigated due to their synergistic effect [23–25]. Pseudocapacitive performance of PANI was modified by distribution of molybdenum oxide in 3D polymer matrix of PANI in our previous work [26]. The obtained PANI/MoO_x composite displayed pseudocapacitive behaviors over an extended potential range of −0.6 to 0.6 V. Composite film of WO_3 and PANI was obtained through depositions of WO_3 and PANI in cathodic and anodic pulses [27]. The obtained film exhibited modified electrochromic properties and the stability of WO_3 was also improved through immobilizing the oxide in the polymer matrix. We have recently demonstrated the electrocodeposition of PANI and WO_3 by cyclic voltammetry and PANI/WO_3 composite film showed good catalytic activities to iodate electrochemical reduction [20]. In this paper, we studied the pseudocapacitive properties of WO_3/PANI composite films electrodeposited by cyclic voltammetry in solutions of aniline and precursor of the oxide prepared from tungstic acid and H_2O_2. The obtained WO_3/PANI composite was characterized by X-ray photoelectron spectroscopy (XPS) and scanning electron microscopy (SEM). The charge storage characteristics were investigated by constant charge–discharge experiments and electrochemical impedance spectroscopy (EIS). An asymmetric model capacitor was assembled by using WO_3/PANI composite and PANI as negative and positive electrodes, respectively.

2. Experimental

Aniline was distilled under reduced pressure prior to use. All other chemicals were analytical grade and used as received. Carbon cloth was purchased from SGL (Germany). The electrochemical experiments were performed by using a multi-channel potentiostat (VMP3, Bio-Logic-Science Instruments) in a three-electrode electrolytic cell. A saturated calomel electrode (SCE) was used as the reference electrode and a platinum plate (ca. 1 cm^2) as the counter electrode. Carbon cloth with geometric area of 0.78 cm^2 was used as the working electrode. All potentials are relative to the SCE.

WO_3/PANI composite films were electrochemically deposited on carbon cloth by using cyclic voltammetry (CV) between −0.6 and 0.9 V at a scan rate of 50 mV s^{-1}. Before electrodeposition, carbon cloth was pre-cleaned by acetone and distilled water, and then pretreated by three cyclic voltammetric scans at 100 mV s^{-1} between −1.5 and 1.5 V in 2 M H_2SO_4. The deposition solution was freshly prepared by tungstic acid (0.15 M), H_2SO_4 (0.5 M) and H_2O_2 (0.0–0.35 M) with stirring at 37 °C for 0.5 h, then aniline was introduced to the above solution (0.075 M). WO_3/PANI composite films electrodeposited by 100 cyclic voltammetric scans from solutions prepared by adding H_2O_2 into the solution (the H_2O_2 concentration is 0, 0.04, 0.08, 0.17 and 0.34 M, respectively in the solution) were denoted as WP^{0M}, $WP^{0.04M}$, $WP^{0.08M}$, $WP^{0.17M}$ and $WP^{0.34M}$, respectively. The film obtained by 25 cyclic voltammetric scans from solution containing 0.08 M H_2O_2 was named as WP^{25c}. Pure WO_3 film was prepared by 25 cyclic voltammetric scans between −0.6 and 0.9 V in a solution freshly prepared by tungstic acid (0.15 M), H_2SO_4 (0.5 M) and H_2O_2 (0.08 M) with stirring at 37 °C for 0.5 h. Aniline electropolymerization was conducted in a solution of aniline (0.075 M) and H_2SO_4 (0.5 M) between −0.2 and 0.9 V to prepare pure PANI film. WO_3, PANI and WO_3/PANI composite (WP) films with different mass were prepared similarly by controlling the cyclic voltammetric scans. The freshly electrodeposited films were washed thoroughly with distilled water and dried in vacuum at room temperature for 24 h. The loading of the films was measured by the weight difference of the electrode (vacuum dried at room temperature) before and after electrodeposition, using Sartorius BT 25 S semi-microbalance with an accuracy of 0.01 mg.

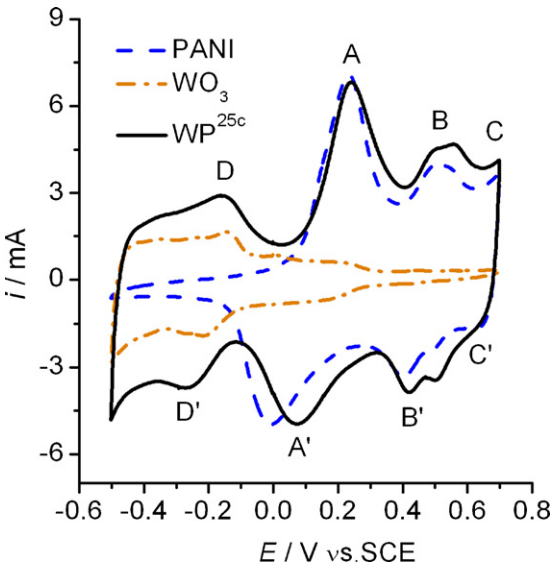

Fig. 1. Cyclic voltammograms of WP^{25c}, PANI and WO_3 films in 1 M H_2SO_4. Scan rate, 10 mV s^{-1}.

The pseudocapacitive behaviors of the films were studied by CV and chronopotentiometry (CP) in 1 M H_2SO_4 electrolyte. The morphologies of the samples were investigated by SEM (LEO SUPRA 35). XPS spectra were recorded on Thermo ECSALAB 250 electron spectrometer using Al Kα radiation (1486.6 eV). EIS spectra were measured on an Impedance Spectrum Analyzer consisted of a 273A Potentiostat/Galvanostat and a 5210EC Lock-In Amplifier, controlled by electrochemical impedance software Power Sine. The potential amplitude of AC was kept at 5 mV, while the composite electrode was subjected to applied DC potentials of −0.5, −0.25, 0.25, 0.5 and 0.7 V, respectively for EIS measurements in a frequency range of 40 kHz–100 mHz. A Luggin capillary was used to minimize errors due to *iR* drop of the electrolyte. The impedance spectra were analyzed by using simulated program of ZSimpWin V3.10.

3. Results and discussions

3.1. Electrodeposition and characterization of WO_3/PANI composite film

Fig. 1 shows the cyclic voltammograms of pure PANI, WO_3 and the composite film WP^{25c} in 1 M H_2SO_4. The cyclic voltammo-

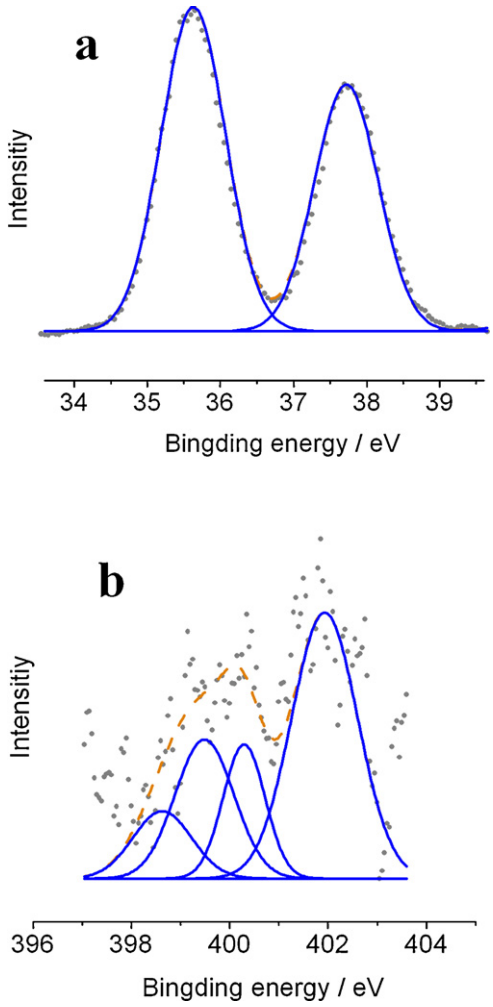

Fig. 2. XPS spectra of W 4f (a) and N 1s (b) for WP^{25c} on carbon cloth.

gram of WP^{25c} has typical redox peaks of PANI (A/A′, B/B′ and C/C′) and WO_3 (D/D′), which indicates that WO_3/PANI composite film is obtained successfully and it possesses activities of both PANI and WO_3. The redox pairs A/A′ and C/C′ are originated from exchanges between leucoemeraldine and emeraldine, emeraldine and pernigraniline states of PANI, respectively. The redox pair B/B′ can be ascribed to hydrolysis products of PANI due to over-oxidation at comparatively high potential [28]. The redox pair D/D′ is due to the tungsten oxide-related redox process, involving the intercalation/deintercalation of protons and electrons into/out of the film, leading to non-stoichiometric hydrogen tungsten bronze or substoichiometric anhydrous tungsten oxide [18].

Surface measurements by XPS are carried out for WP^{25c} to verify the chemical composition of composite film. The XPS core level spectra of W 4f and N 1s are shown in Fig. 2. In the spectrum of W 4f (Fig. 2a), the peaks appearing at 35.57 and 37.9 eV can be assigned to W $4f_{7/2}$ for W^{+6} oxidation state (i.e.WO_3 species) [29,30]. Fig. 2b shows N 1s XPS spectrum of WP^{25c}. The N 1s core level can be deconvoluted into four peaks. The binding energy centered at 398.6 and 399.5 eV can be assigned to the quinoid imine [=N–] and the benzenoid amine [–NH–]. The binding energy >400 eV can be ascribed to the positively charged nitrogen [N^+] [31], in which the peak at 400.3 and 401.9 eV are associated with the cationic nitrogen atoms (=NH^+) and the protonated amine units (–NH^+) in PANI [32].

Different surface morphologies of pure PANI, WO_3 and WP^{25c} films on carbon cloth are clearly shown in Fig. 3. It can be seen that

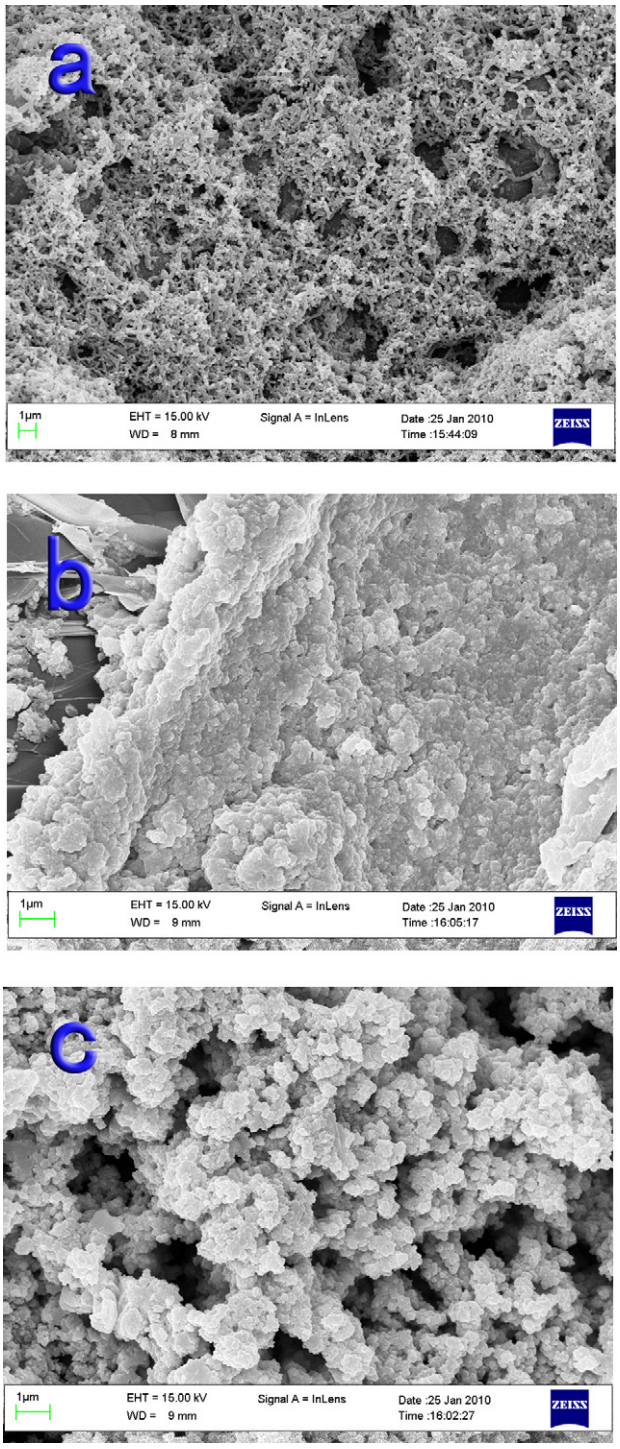

Fig. 3. SEM images of PANI (a), WO_3 (b) and WP^{25c} (c) on carbon cloth.

PANI film displays nano-fibrous structure with many open porosities. WO_3 film is composed of fused large particles. While the WP^{25c} film displays rough porous surface of micro aggregates with a larger active surface area than that of pure WO_3. This micro porous structure with high specific area may provide more opportunity for the reactive centers on the film to contact with electrolyte and so facilitate the charge transfer in the bulk of the film. This is in agreement with the CV results (Fig. 1) that the peak currents corresponding to the redox processes of tungsten oxide in the cyclic voltammogram of WP^{25c} (D/D′) are much higher than those of pure WO_3.

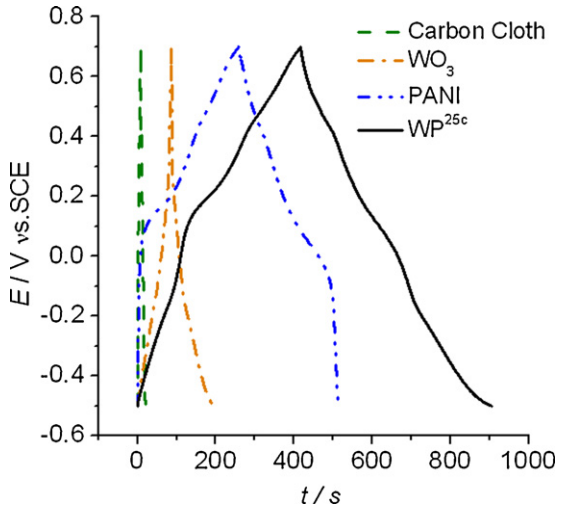

Fig. 4. Charge–discharge curves of WP^{25c}, PANI and WO_3 films measured in 1 M H_2SO_4 between −0.5 and 0.7 V at 1.28 mA cm^{-2}.

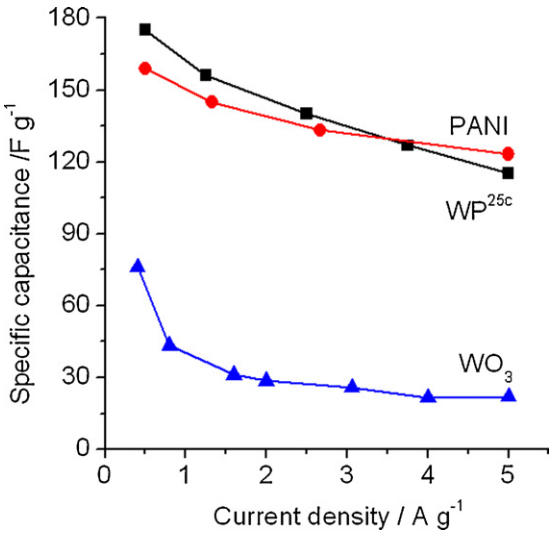

Fig. 5. Dependence of the specific capacitance of PANI, WO_3 and WP^{25c} on current density.

3.2. Capacitive performance of WO_3/PANI composite film

It can be observed from Fig. 1 that WP^{25c} film exhibits reversible redox transitions over the potential range of −0.5 to 0.7 V. The almost immediate reversal of current response at the switching potential reveals that WO_3/PANI composite film has pseudocapacitive characteristics over a wide potential range of 1.2 V [33].

The galvanostatic charge–discharge measurements by CP were carried out on these films and the substrate of the films, carbon cloth in 1 M H_2SO_4 at 1.28 mA cm^{-2} (Fig. 4). The potential responses of the composite film during charge and discharge are nearly symmetrical and the working potential window can be extended to 1.2 V which is wider than those of pure PANI and WO_3. The specific capacitance (C_s) of WP^{25c} is 168 F g^{-1} and the energy density (E_s) is 33.6 Wh kg^{-1} which increases 91% compared with that of PANI (17.6 Wh kg^{-1}) due to the capacitance contributed from the participation of WO_3 particles. The carbon cloth displays a specific capacitance of 0.3 F g^{-1}, indicating that the substrate has little contribution to the specific capacitance of the composite film. The energy density of WP^{25c} is comparable to those of other PANI-based composite, such as PANI/MnO_2 (24.2 Wh kg^{-1}) and PANI/Multiwalled carbon nanotube (33.5 Wh kg^{-1}) [34,35]. However, WP^{25c} possesses high energy storage capacity in both positive and negative potential range and thus can be used as both positive and negative electrodes in supercapacitors.

The dependence of the specific capacitance of PANI, WO_3 and WP^{25c} on charge–discharge current density was displayed in Fig. 5. The capacitance of WO_3 significantly decreases with charge–discharge current density increasing. Its specific capacitance at charge–discharge current density of 5 A g^{-1} is only ca. 29% of that at 0.5 A g^{-1}, which is improved by incorporation of PANI with WO_3 to form WP^{25c} due to the distribution of WO_3 particles in the network of PANI. The capacitance of WP^{25c} can be retained about 66% with the increasing of the charge–discharge current density from 0.5 to 5 A g^{-1}.

Fig. 6 presents the specific capacitance of WO_3, PANI and WO_3/PANI composite (WP) with different mass of films. With the mass of films increasing, the specific capacitance of WO_3 decreases by 5.3%, corresponding to 4 F mg^{-1}. This is probably because of the diffusion limitation in the WO_3 dense film (Fig. 3). Due to the distribution of WO_3 in the PANI network, WO_3/PANI composite displays a decrease of only 0.9% in the specific capacitance, corresponding to 1.6 F mg^{-1} with the mass of film increasing from 2.4 to 8.1 mg. This implies that the Faradic reaction takes place not only at the surface but also in the bulk of the film.

The constant current charge–discharge cycling performance of these films were also investigated over the potential range of −0.5 to 0.7 V at current density of 1 A g^{-1} in 1 M H_2SO_4 (Fig. 7). The capacitance of WO_3 sharply decreases upon charge–discharge cycling and more hydrogen evolves after 210 cycles. Upon distribution of WO_3 particles in the network of PANI, although the cycling stability needs further improvement, the charge–discharge cycling is prolonged. The specific capacitance of WP^{25c} decreases from 166 F g^{-1} in the initial to 99 F g^{-1} after 1000 cycles, which may be due to the intense interaction (such as hydrogen bond) between WO_3 and PANI [20,36].

3.3. Influence of H_2O_2 on electrodeposition of WO_3/PANI composite film

To investigate the influence of H_2O_2 on the deposition of WO_3/PANI composite films, WP^{0M}, $WP^{0.04M}$, $WP^{0.08M}$, $WP^{0.17M}$ and $WP^{0.34M}$ were electrodeposited from solutions containing 0, 0.04,

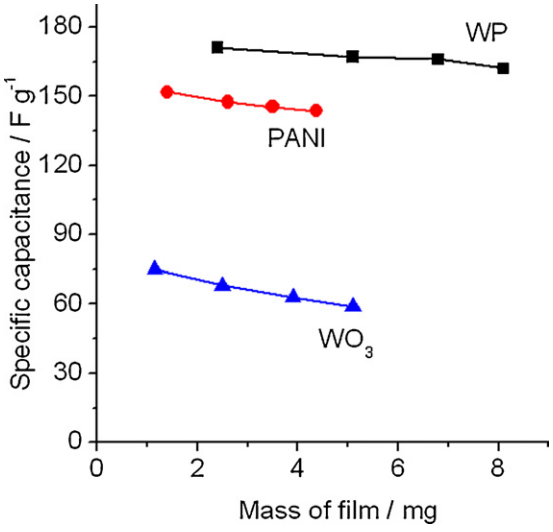

Fig. 6. The specific capacitance of PANI, WO_3 and the composite WP as a function of the film mass measured through constant current charge–discharge at 1 A g^{-1} in 1 M H_2SO_4.

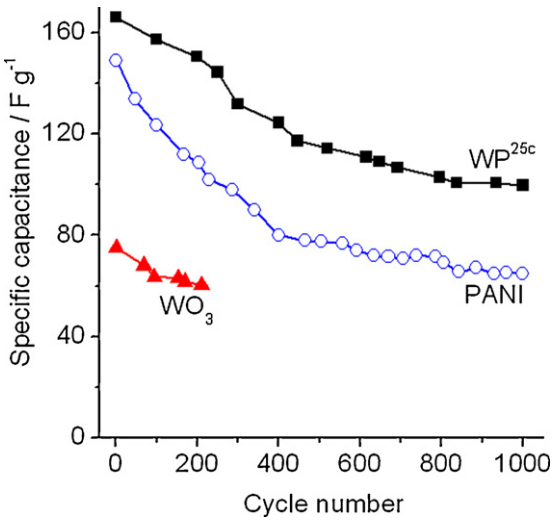

Fig. 7. Cycling performance of PANI, WO_3 and WP^{25c} films measured through constant current charge–discharge at 1 A g^{-1} over potential range of −0.5 to 0.7 V in 1 M H_2SO_4.

0.08, 0.17 and 0.34 M of H_2O_2, respectively through 100 cyclic voltammetric scans. The obtained films were studied by CV and CP. Fig. 8 shows the cyclic voltammograms of the composite films. It can be found that the tungsten oxide-related redox peak currents increase with increasing H_2O_2 concentration (inset of Fig. 8), which suggests that the addition of H_2O_2 benefits the electrodeposition of WO_3. This is mainly attributed to the formation of peroxo-precursors in the deposition solution from tungsten acid and H_2O_2 [19]. The peroxy-tungstate is assumed to undergo electrochemical reduction and give rise to WO_3 on the substrate. It has been reported that the electrochemical deposition of WO_3 from peroxy-tungstate is more favorable on the substrate than from poly-tungstate [19,37]. Moreover, H_2O_2 is also a stabilizer and complex reagent for the formation of homogenous solutions by preventing tungsten oxide from aggregation in the extended period [19]. The PANI-related redox peak currents on the CV curves

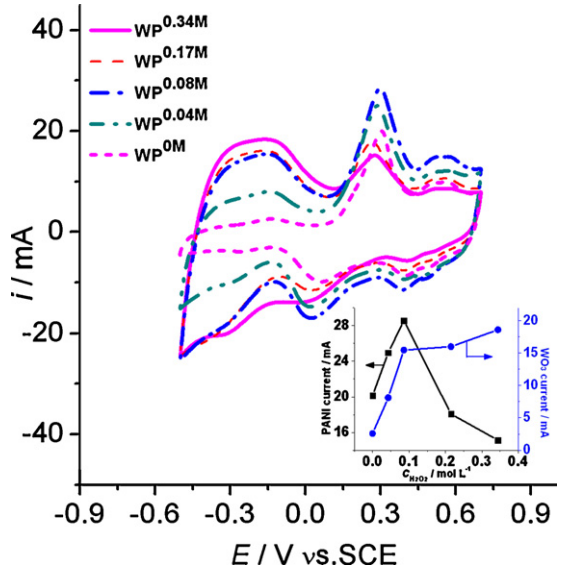

Fig. 8. Cyclic voltammograms of the composite films obtained from solutions containing 0 (WP^{0M}), 0.04 ($WP^{0.04M}$), 0.08 ($WP^{0.08M}$), 0.17 ($WP^{0.17M}$) and 0.34 M H_2O_2 ($WP^{0.34M}$). Inset shows PANI-related (black line) and WO_3-related (blue line) anodic peak currents on the CVs of the films made from solutions containing H_2O_2 in different concentrations.

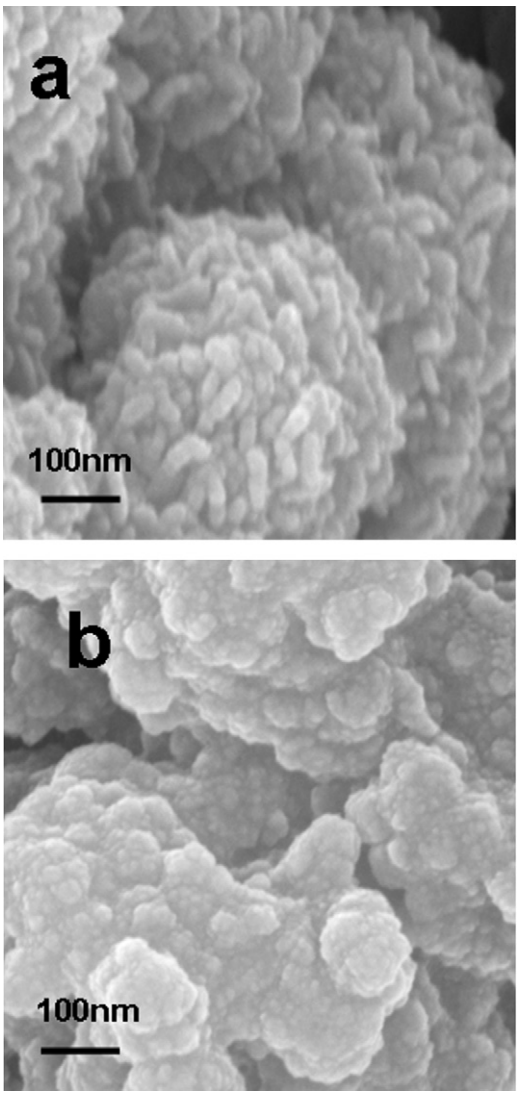

Fig. 9. SEM images of the composite films of $WP^{0.08M}$ (a) and WP^{0M} (b).

increase with the increase of H_2O_2 concentration up to 0.08 M and then begin to decrease when more H_2O_2 is added in the solution (Fig. 8). This may be due to the chemical polymerization of aniline in the presence of excess of H_2O_2 in the solution and hence restrain the electrochemical growth of PANI on the substrate [38]. The surface morphology of WO_3/PANI composite film is changed by adding H_2O_2 into the deposition solution (Fig. 9). In comparison to WP^{0M} composite film (Fig. 9(b)), $WP^{0.08M}$ shows a cluster-like microstructure formed by aggregated nanoparticles (Fig. 9(a)). The CP measurement results show that $WP^{0.08M}$ composite film made from solution containing 0.08 M H_2O_2 exhibits the highest specific capacitance among the films (Fig. 10), which is in agreement with the CV results.

3.4. EIS of WO_3/PANI electrode

Electrochemical impedance characteristics of the $WP^{0.08M}$ composite film were investigated at applied dc potentials of −0.5, −0.25, 0.25, 0.5 and 0.7 V, respectively. The Nyquist diagrams in the range of 40 kHz to 100 mHz are shown in Fig. 11. There is a semicircle impedance arc in the high frequency region on all the curves, while only a small part of the circle in the impedance arc is obtained at −0.25 and −0.5 V. This semicircle is attributable to the process at the composite–electrolyte interface, which is expected to be the

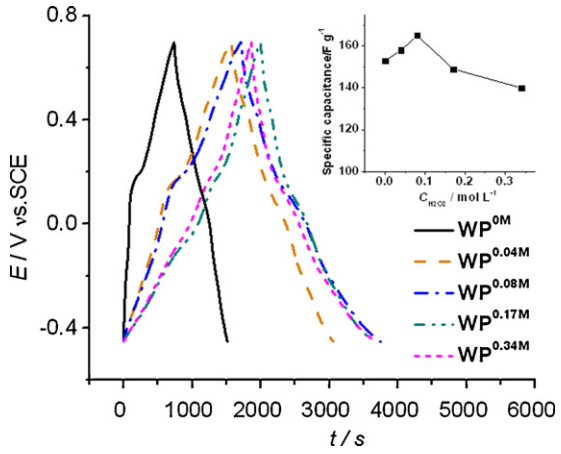

Fig. 10. Constant current charge–discharge curves of WP^{0M}, $WP^{0.04M}$, $WP^{0.08M}$ $WP^{0.17M}$ and $WP^{0.34M}$ at 1.28 mA cm^{-2} in 1 M H_2SO_4. Inset shows specific capacitances of the films.

double-layer capacitance (C_{dl}) in parallel with the charge-transfer resistance (R_{ct}) due to the charge exchange and compensation at the composite–solution interface [39]. A slope of a nearly vertical line arises in the low frequency region on the curves due to the faradic pseudocapacitance (C_F) of the composite film. An equivalent circuit corresponding to the impedance responses is in inset A of Fig. 11, in which R_Ω represents the uncompensated electrical resistance, including those of the electrode active material (R_a), the electrolyte (R_e) and the electrical leads combined (R_l) [39].

The fitting values of the equivalent circuit elements are in Table 1 and the dependence of some impedance parameters on potential is in inset B of Fig. 11. The mean error of modulus is less than 1%, implying that the parameter values obtained from EIS fitting via such proposed circuit are reliable. The values of R_e and R_l are almost not influenced by the applied potential, so the difference in R_Ω induced by the applied potential should be resulted from the difference in R_a. The smallest R_Ω at −0.5 V can be ascribed to the increased conductivity of the composite due to the formation of tungsten bronze at this potential. The R_{ct} shows a large value of 0.544 Ω at 0.7 V (Table 1 and inset B of Fig. 11), indicating that it

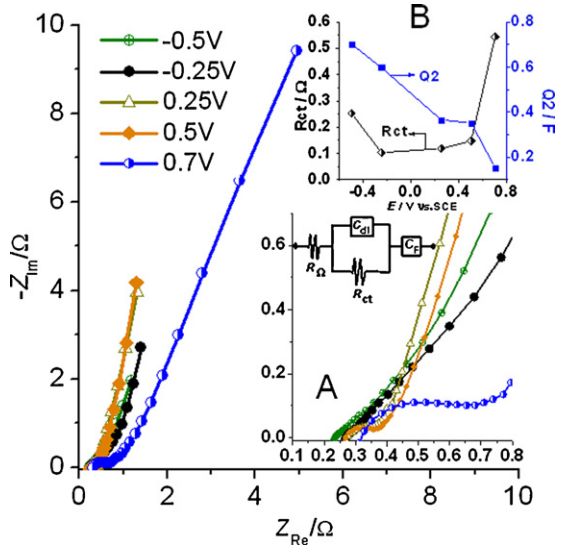

Fig. 11. Impedance spectra in the range of 40 kHz to 100 mHz of $WP^{0.08M}$ measured at different DC potential in 1 M H_2SO_4. Insets are the expansion of impedance spectra, corresponding equivalent circuit (A) and some impedance parameters *vs.* potential (B).

Table 1
The best fitting values of the equivalent circuit elements in inset A of Fig. 11 for the impedance data.

Potentials (V)	R_Ω (Ω)	Q_1 (F)	n_1	R_{ct} (Ω)	Q_2 (F)	n_2	Error (%)
−0.5	0.238	0.587	0.579	0.253	0.703	0.768	0.84
−0.25	0.272	0.473	0.542	0.103	0.598	0.912	0.50
0.25	0.276	0.059	0.657	0.119	0.366	0.835	0.37
0.5	0.271	0.060	0.573	0.148	0.352	0.831	0.54
0.7	0.294	0.019	0.536	0.544	0.154	0.739	0.58

is more difficult for the charge exchange and compensation at the composite–solution interface at this potential. This R_{ct} (0.544 Ω) and the comparatively higher R_Ω (0.294 Ω) can be attributable to the low conductivity of WO_3 at this high positive potentials [27]. Due to the porous surface of electrodes, constant phase elements CPE1 and CPE2 are used to express C_{dl} and C_F in the equivalent circuit. The impedance of the constant-phase element is defined as $Z_{CPE} = [Q(j\omega)^n]^{-1}$ with $-1 \le n \le 1$, where Q, ω and n are the frequency-independent constant representing capacitance, angular frequency and a correction factor between 0 and 1, respectively [40]. The value of n_2 is between 0.7 and 1 indicating the porous nature of the electrode. The value of Q_2 is higher at negative potentials (inset B of Fig. 11), implying that the composite film is more suitable to be used as negative electrode for the capacitors.

3.5. Asymmetric capacitor performance

As $WP^{0.08M}$ is more suitable as negative electrode for the capacitors, an asymmetric PANI(+)/$WP^{0.08M}$(−) capacitor was modeled by using PANI and $WP^{0.08M}$ as positive and negative electrodes, respectively, with 1 M H_2SO_4 as the electrolyte. Due to the high electroactivities of PANI at positive and $WP^{0.08M}$ at negative potentials, pseudocapacitive properties of the asymmetric capacitor are investigated over a wide operating voltage of 1.2 V. Fig. 12 represents cyclic voltammograms of the asymmetric capacitor at scan rates of 5, 10, and 20 mV s^{-1}. The symmetric CV curves reveal that the capacitor has pseudocapacitive characteristic over operating voltage of 1.2 V, which can be also observed from the constant current charge–discharge curves (not shown). In the charging process, PANI on the positive electrode is p-doped and WO_3 on the negative electrode is n-doped.

The rate performance of the asymmetric capacitor examined at various current rates is shown in Fig. 13. It reveals

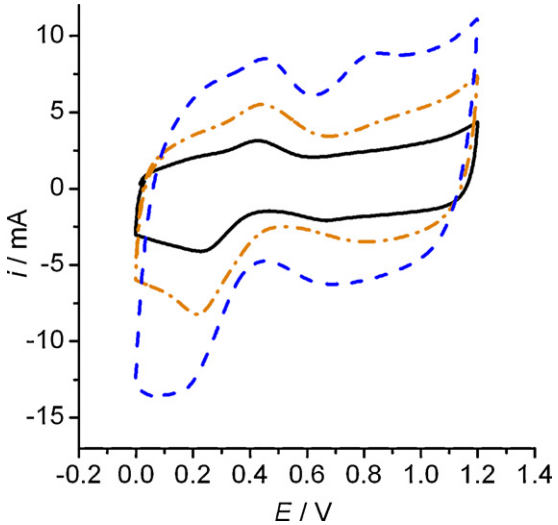

Fig. 12. Cyclic voltammograms of asymmetric capacitor based on PANI and $WP^{0.08M}$ electrodes in 1 M H_2SO_4 over operating voltage of 1.2 V at 5, 10, and 20 mV s^{-1}.

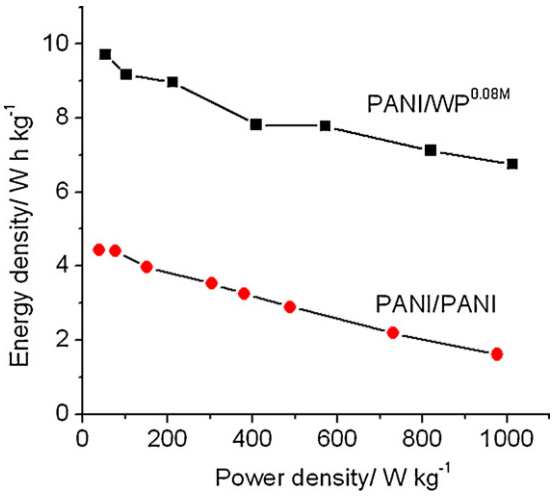

Fig. 13. Ragone plots of asymmetric PANI(+)/$WP^{0.08M}$(−) capacitor over operating voltage of 1.2 V and symmetric PANI(+)/PANI(−) capacitor over operating voltage of 0.7 V.

that the asymmetric PANI(+)/$WP^{0.08M}$(−) capacitor has much higher energy density than that assembled with two PANI electrodes, which is mainly attributed from the larger operating voltage of PANI(+)/$WP^{0.08M}$(−) capacitor (1.2 V) than that of capacitor assembled with two PANI electrodes (0.7 V). Meanwhile, PANI(+)/$WP^{0.08M}$(−) capacitor keeps a good rate capability due to its large surface area and low charge transfer resistance. The energy density E_s of the asymmetric capacitor is found to be 9.72 Wh kg^{-1} at the power density P of 53 W kg^{-1}, calculated by the equation $E_s = 1/2C_sV^2$ and $P = E_s/t$, where C_s is the specific capacitance based on the active materials on two electrodes, V is the operating voltage of the cell and t is the discharge time obtained by chronopotentiometry. For comparison, the energy density of the symmetric capacitor assembled with two PANI electrodes is 4.5 Wh kg^{-1} at 50 W kg^{-1}.

4. Conclusion

WO_3/PANI composite films exhibited good pseudocapacitive performance in a wide potential range of −0.5 to 0.7 V *vs.* SCE due to the electroactivities of WO_3 in negative potential range and its fine distribution in PANI matrix. It has been shown that a small addition of H_2O_2 in the deposition solution facilitated the deposition of tungsten oxide and thus led to the enhanced energy storage capabilities of the composite film, especially in the negative potential range. An asymmetric model capacitor assembled with WO_3/PANI and PANI as negative and positive electrodes can be operated over a large working voltage of 1.2 V and displayed an energy density two times higher than that of a symmetric capacitor modeled by using two PANI films as both positive and negative electrodes. This work demonstrates that the low-cost and benign environment of WO_3/PANI can be a promising negative electrode material for asymmetry capacitors.

Acknowledgements

This work was supported by National Natural Science Foundation of China (project number 50973013), Open Projects of State Key Laboratory of Supramolecular Structure and Materials (SKLSSM 201002), and Key Laboratory of Functional Inorganic Material Chemistry (Heilongjiang University), Ministry of Education.

References

[1] C. Peng, S. Zhang, D. Jeweel, Prog. Nat. Sci. 18 (2008) 777.
[2] S. Sarangapani, B.V. Tilak, C.-P. Chen, J. Electrochem. Soc. 143 (1996) 3791.
[3] A.A. Anani, US005549989-A.
[4] J.-K. Lee, H.M. Pathan, K.-D. Jung, J. Power. Sources 159 (2006) 1527.
[5] S.G. Kandalkar, J.L. Gunjakar, C.D. Lokhande, Appl. Surf. Sci. 254 (2008) 5540.
[6] Y.-Z. Zheng, H.-Y. Ding, M.-L. Zhang, Mater. Res. Bull. 44 (2009) 403.
[7] G. Lota, E. Frackowiak, J. Mittal, Chem. Phys. Lett. 434 (2007) 73.
[8] J.-K. Chang, C.-H. Huang, W.-T. Tsai, Electrochim. Acta 53 (2008) 4447.
[9] V. Gupta, N. Miura, Mater. Lett. 60 (2006) 1466.
[10] M. Hughes, M.S.P. Shaffer, A.C. Renouf, Adv. Mater 14 (2002) 382.
[11] V. Khomenko, E.R. -Pinero, F. Beguin, J. Power Sources 177 (2008) 643.
[12] A. Malak, K. Fie, G. Lota, J. Solid State Elecrochem. 14 (2010) 811.
[13] A.J. Rudge, J.P. Ferraris, S. Gottesfeld, US5527640A.
[14] A. Laforgue, P. Simon, C. Sarrazin, J. Power Sources 80 (1999) 142.
[15] L. Li, D.C. Loveday, D.S.K. Mudigonda, J. Electrochem. Soc. 149 (2002) A1201.
[16] A.M. Timinov, S.A. Loginov, N. Shkolnik, WO2003065536-A2.
[17] J.R. Owen, K.M. Brace, WO2005101548-A1.
[18] P.J. Kulesza, L.R. Faulkner, J. Am. Chem. Soc. 110 (1988) 4905.
[19] T. Pauporte, J. Electrochem. Soc. 149 (2002) C539.
[20] B.-X. Zou, X.-X. Liu, D. Diamond, Electrochim. Acta 55 (2010) 3915.
[21] Y.U. Jeong, A. Manthiram, J. Electrochem. Soc. 148 (2001) A189.
[22] C.-C. Huang, W. Xing, S.-P. Zhuo, Scripta Mater. 61 (2009) 985.
[23] A.M. Murugan, A.K. Viswanath, C.S. Gopinath, J. Appl. Phys. 100 (2006) 074319.
[24] L.-J. Sun, X.-X. Liu, K.K.-T. Lau, Electrochim. Acta 53 (2008) 3036.
[25] P.G. Romero, M. Chojak, K.C. Gallegos, Electrochem. Commun. 5 (2003) 149.
[26] X.-X. Liu, L.-J. Bian, L.-J. Zhang, J. Solid State Electrochem. 11 (2007) 1279.
[27] P.K. Shen, H.T. Huang, A.C.C. Tseung, J. Electrochem. Soc. 139 (1992) 1840.
[28] H.-F. Jiang, X.-X. Liu, Electrochim. Acta 55 (2010) 7175.
[29] M.R. Field, D.G. McCulloch, S.N.H. Lim, J. Phys.: Condens. Matter 20 (2008) 175216.
[30] J. Zhang, J.P. Tu, X.H. Xia, Sol. Energy Mater. Sol. Cells 93 (2009) 1840.
[31] M.G. Han, S.S. Im, Polymer 41 (2000) 3253.
[32] X.-L. Wei, M. Fahlman, A.J. Epstein, Macromolecules 32 (1999) 3114.
[33] B.E. Conway, V. Birss, J. Wojtowicz, J. Power Sources 66 (1997) 1.
[34] L. Chen, L.-J. Sun, F. Luan, J. Power Sources 195 (2010) 3742.
[35] V. Khomenko, E. Frackowiak, F. Beguin, Electrochim. Acta 50 (2005) 2499.
[36] A. Tiwari, S. Gong, Electroanalysis 20 (2008) 1775.
[37] E.A. Meulenkamp, J. Electrochem. Soc. 144 (1997) 1664.
[38] H. Ding, M. Wan, Y. Wei, Adv. Mater. 19 (2007) 465.
[39] Y.-K. Zhou, B.-L. He, W.-J Zhou, H.-L. Li, J. Electrochem. Soc. 151 (2004) A1052.
[40] T.C. Girija, M.V. Sangaranarayanan, J. Power Sources 156 (2006) 705.